Differential scanning calorimetric x-ray diffraction and spectroscopic studies of phase transitions in the bidimensional compound $(C_9H_{19}NH_3)_2PbCl_4$

1996 J. Phys.: Condens. Matter 8 8465

(http://iopscience.iop.org/0953-8984/8/44/003)

J. Phys.: Condens. Matter **8** (1996) 8465–8475. Printed in the UK

Differential scanning calorimetric x-ray diffraction and spectroscopic studies of phase transitions in the bidimensional compound $(C_9H_{19}NH_3)_2PbCl_4$

S Kammoun†, M Kamoun†, A Daoud† and A Lautie‡

† Departement de Physique, Laboratoire de l'Etat Solide, Faculté des Sciences de Sfax, Route de Souka Km 3, 3038 Sfax, Tunisia

‡ Laboratoire de Spectrochimie Infrarouge et Raman, CNRS, 2 rue Henry Dunant, 94320, Thiais, France

Received 14 June 1996

Abstract. Four crystalline phases (called III, II, II′ and I) have been observed in the perovskite-type layer compound $(C_9H_{19}NH_3)_2PbCl_4$ using differential scanning calorimetry, x-ray diffraction and spectroscopic studies. The crystallographic evolution with increasing temperature appears to be triclinic III → monoclinic II → monoclinic I. An intermediate disordered phase II′, stable in a narrow temperature range and structurally similar to phase II, has also been observed, such that the transformation II → I proceeds, in fact, two steps II → II′ → I. Phase III, stable at low temperature, has an ordered structure. The phase transition III → II, which is of first-order type, corresponds to an order–disorder mechanism involving the organic part of the structure (alkylammonium chains) and deformation of $PbCl_6$ octahedra. The phase transition II → II′, which is of second-order type, is related to the arrangement of $PbCl_6$ octahedra of perovskite layers. The II′ → I transition is of first-order type and involves conformational disorder of the chains. In phase I chain melting sets in.

1. Introduction

The tetrahalometallates of bis(*n*-alkylammonium) of general formula $(C_nH_{2n+1}NH_3)_2MX_4$ where M = Cd, Pb, Mn, Cu, Fe, Pd, ... and X = Cl, Br are known to crystallize in a bidimensional structure of perovskite type (Chapuis *et al* 1975, Depmeier 1977, Kind *et al* 1979). The general structure of these materials, as shown schematically in figure 1, consists of layers of corner-sharing (MX_6^{2-}) octahedra alternating with compact layers formed from *n*-alkylammonium ions. The NH_3 polar heads of the *n*-alkylammonium groups are linked to the chlorine matrix by three NH ... Cl hydrogen bonds with two axial chlorine atoms and one equatorial chlorine atom; this configuration is called monoclinic and is the only one allowed for steric reasons when $n \geqslant 2$ (Depmeier 1977). The metallic sheets are bound by both Van der Waals interactions between the CH_3 alkyl ends and Coulomb forces between the positively charged organic ions and the negatively charged octahedra. These compounds present interesting magnetic and structural properties. In particular, they exhibit several structural phase transitions governed by the dynamics of the alkylammonium ions and by the 'rotations' of the MX_6 octahedra about the three crystallographic axes. The structural phase transitions related to the alkylammonium ions have been divided into two classes: (i) order–disorder transitions connected with reorientational motions of the rigid alkylammonium chains about their long axes monitored by flippings of NH_3 polar heads between two or

0953-8984/96/448465+11$19.50

more potential wells in the cavities and (ii) conformational transitions. This second type exists only if the number of carbon atoms is large enough ($n > 3$). It involves cooperative conformational changes in the chains, which is defined as the rapid diffusion of one or more *gauche* bonds up and down the chain, and leads to a 'quasi-melting' of the hydrocarbon part of the chains while the metallic sheets play the part of elastic stable matrices. This behaviour shows analogies with that of liquid crystals and lipid bilayer membranes.

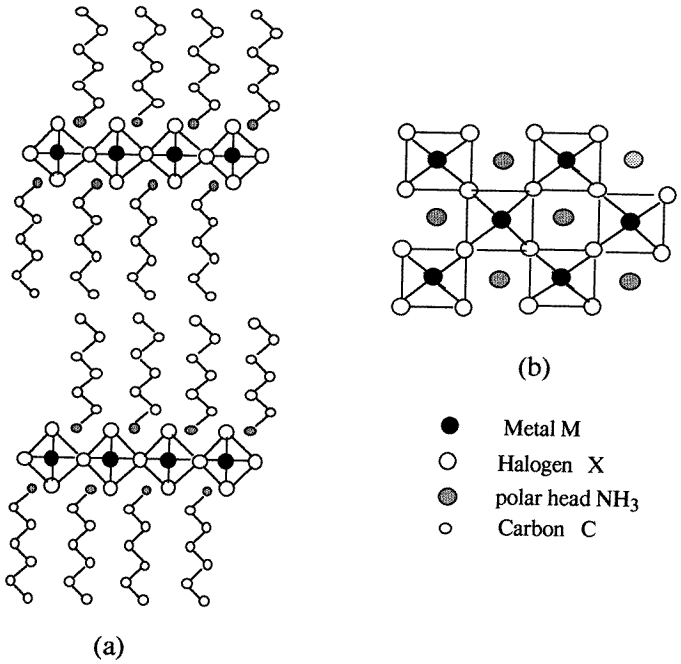

Figure 1. (a) The schematic structure of compounds with general formula $(C_nH_{2n+1}NH_3)_2MX_4$. (b) A projection of the ideal structure in the mineral plane.

In the series of lead compounds $(C_nH_{2n+1}NH_3)_2PbCl_4$ (short notation C_nPb) first results were published by Abid *et al* in the case of the C_3Pb compound (Abid *et al* 1990, 1992, Romain *et al* 1992).

The aim of the present work is to study the polymorphic behaviour of the C_9Pb compound from the results of calorimetric analysis, x-ray diffraction and infrared and Raman spectroscopies.

2. Experimental section

2.1. Preparation

The compound has been prepared by mixing *n*-alkylammonium chloride (prepared by HCl on the corresponding amine) and lead chloride, in stoichiometric proportions, according to the reaction

$$2(C_9H_{19}NH_3Cl) + PbCl_2 \rightarrow (C_9H_{19}NH_3)_2PbCl_4.$$

The product crystallizes as very small platelets.

2.2. Differential scanning calorimetry

Calorimetric measurements were performed on a Perkin–Elmer differential scanning calorimetric series 7. The thermal recording conditions were as follows: temperature speeds (heating or cooling) of 1 K min^{-1}; temperature range from 253 to 323 K and sensitivity of 5 mV mW^{-1}.

2.3. X-ray diffraction

X-ray powder diffraction experiments were carried out with an Enraf–Nonius Guinier–Simon camera. Working in transmission allows crystallographic changes as a function of temperature to be recorded on the photographic diffraction pattern. The experimental conditions were as follows: heating rates of 0.4 K min^{-1}; CuKα radiation, quartz monochromator; x-ray window width of 1 mm, film speed of 1 mm h^{-1}, x-ray generator power of 1 kW, temperature range from 113 to 353 K.

2.4. Raman and infrared spectroscopies

Raman spectra were recorded using a DILOR RTI 30 triple monochromator equipped with holographic gratings and interfaced to an Interdata minicomputer. The excitation was 514.5 nm from a Spectra-Physics 164 argon ion laser with a power less than 400 mW. The resolution is $\sim$1–2 cm^{-1}. The powdered compound, in a sealed glass cell, is introduced in a Meric cryostat, operating from 193 to 320 K using a continuous flow of helium gas. The sample temperature was measured with a Au(Fe 0.07%)–chromel thermocouple. For the infrared experiments, we did not use the usual KBr pellets to avoid any extra effects of pressure on chemical exchange. Spectra were performed as Nujol mulls squeezed between CsI or CaF_2 windows. Infrared spectra were recorded on a Perkin–Elmer 983 spectrometer using a conventional cell from 90 to 313 K.

3. Evidence of phase transitions by diffraction and calorimetric measurements

3.1. X-ray diffraction

Two crystalline phase transitions clearly appear at 283 and 312 K on the Guinier–Simon pattern (figure 2) recorded while increasing the temperature. So three crystalline phases can be defined:

- a low-temperature phase, called III, stable below 283 K
- a middle-temperature phase, called II, stable between 283 and 312 K
- a high-temperature phase, called I, stable above 312 K.

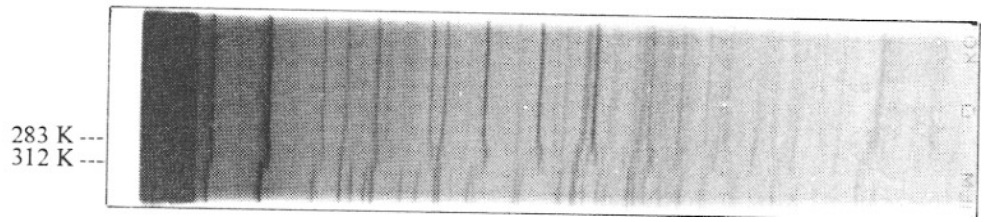

Figure 2. The Guinier–Simon diffraction pattern of $(C_9H_{19}NH_3)_2PbCl_4$.

On the Guinier–Simon diagram obtained with increasing temperature the first transition III → II is revealed only by a slight modification in the positions of the diffraction lines whereas at the second transition II → I the positions and intensities change discontinously.

Table 1. The three sets of crystal data of phases III, II and I of C_9Pb.

	III (223 K) triclinic	II (300 K) monoclinic	I (353 K) monoclinic
a (Å)	7.826(3)	7.757(2)	7.803(3)
b (Å)	7.763(2)	7.696(1)	7.719(4)
c (Å)	48.07(1)	47.720(8)	49.93(2)
α (°)	97.29(1)	90	90
β (°)	96.99(4)	90.85(4)	99.04(5)
γ (°)	89.70(3)	90	90

Table 2. The interlayer distance, d, of the different phases of C_9Pb.

	III (270 K)	II (300 K)	I (353 K)
d (Å)	23.97	23.85	24.65

The values of the cell parameters are reported in table 1. The parameter c is related to the interlayer distance, and a and b are parallel to the plane of the layers. Table 2 reports the values of the interlayer distance d obtained from the Guinier–Simon pattern.

3.2. Differential scanning calorimetry

The differential scanning calorimetry (DSC) curves observed during heating and cooling processes are presented in figure 3. Three phase transitions are observed; they define the domains of four phases named III, II, II′ and I.

Table 3. Transition temperatures, enthalpies and entropies of C_9Pb obtained through DSC.

		T (K)	ΔH (kJ mol^{-1})	ΔS (J K^{-1} mol^{-1})
Transition III → II	Heating	$T_0^1 = 275$	7.7 ± 0.1	27.9 ± 0.4 (3.3 R)
		$T_s^1 = 276.2$		
	Cooling	$T_0^1 = 267$		
		$T_s^1 = 266$		
Transition II → II′	Heating	$T_0^2 = 301.8$		
		$T_s^2 = 304.7$		
Transition II′ → I	Heating	$T_0^3 = 308.6$	14.6 ± 0.2	47.3 ± 0.7 (5.7 R)
		$T_s^3 = 310.4$		
	Cooling	$T_0^3 = 308.2$		
		$T_s^3 = 306.5$		

Transition temperatures, enthalpies and entropies of C_9Pb are reported in table 3. The transition temperatures are given through the 'onset' temperature T_0 and 'peak' temperature

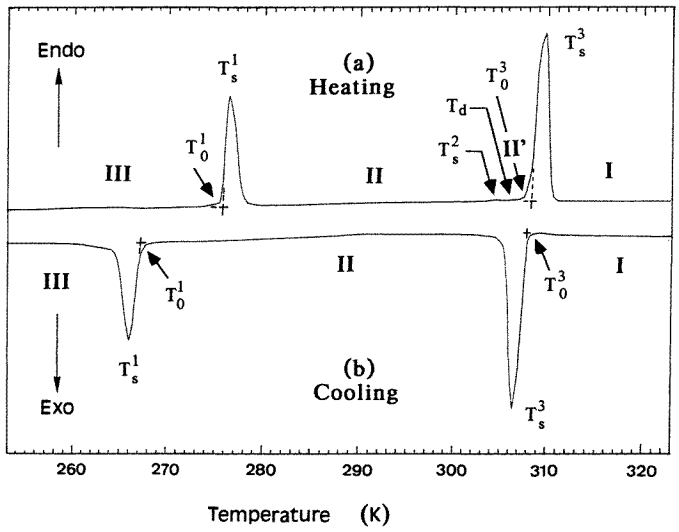

Figure 3. DSC results concerning the phase transitions in $(C_9H_{19}NH_3)_2PbCl_4$.

T_s, and the corresponding enthalpic value was obtained from a signal treatment program. The entropy change computed from the relation $\Delta S = \Delta H/T$ and the number Ω (equivalent position) deduced from the relation $\Delta S = R \log \Omega$ are also reported.

The DSC curves represented in figure 3 show that the transitions III $\rightarrow$ II and II$'$ $\rightarrow$ I are subject to a small hystersis, indicating thus their first-order character. The comparison of the enthalpies ΔH of the transitions shows that the main structural changes are observed at the phase transition II$'$ $\rightarrow$ I. On the heating curve, a deviation of the baseline is detected at 306.2 K (T_d) before an intense endothermic signal characterized by an onset temperature $T_0^3 = 308.6$ K and a peak temperature $T_s^3 = 310.4$ K. A hump with a peak temperature $T_s^2 = 304.7$ K is observed, which seems to reveal the existence of a new crystalline form, called II$'$, in the narrow temperature range between 304.7 and 310.4 K. Thus, the DSC results allows us to conclude that the transition II $\rightarrow$ I proceeds through several steps: a phase transition II $\rightarrow$ II$'$ at 304.7 K with a weak enthalpy variation and a pretransitional effect observed at 306.2 K before a first-order phase transition II$'$ $\rightarrow$ I at 308.6 K. So from DSC and diffraction data, four decrystalline phases can be defined:

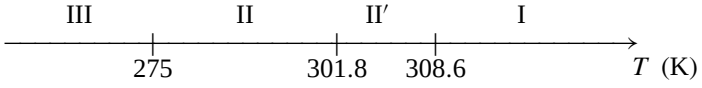

4. Spectroscopic study

4.1. Study of the ordered low-temperature phase III

The vibrational spectra of the low-temperature phase III are studied in order to determine the structure of the alkylammonium chains. Their analysis is necessary to understand the cation dynamics in the disordered phases.

4.1.1. Raman spectra of C_9Pb at 193 K. The so-called lattice vibrations are due to the vibrational modes of the $PbCl_6$ octahedron layers, and to the 'external' vibrations of the alkylammonium cations: they are expected below 360 cm^{-1} (figure 4). The wavenumbers of the observed lattice modes are listed in table 4. We do not intend to give here a detailed assignment, but we intend as far as possible to distinguish between the bands corresponding to the $PbCl_6$ otahedra motions and those associated with $C_9H_{19}NH_3$ chains. To this end we have compared the Raman spectra of C_9Pb at 193 K with the corresponding spectra of the lower homologous compounds C_3Pb (Abid *et al* 1992). The band at 134 cm^{-1} is assigned to the ν(Pb–Cl) mode, whereas the other bands at 28, 48, 117, 168 and 196 cm^{-1} are assigned to the alkylammonium chain motions. The band at 196 cm^{-1} corresponds to a chain libration (Abid *et al* 1992). The longitudinal acoustic mode (LAM-1) wavenumber is characteristic of both length and geometry of chain (Minoni and Zerbi 1982). This mode appears near 245 cm^{-1} (figure 4), which is higher than in the corresponding *n*-alkane, 231 cm^{-1}, as expected for an all-*trans* chain engaged in hydrogen bonds (Mizushima and Simanuti 1949). This suggests that the chain geometry is not entirely extended and represents a *gauche* (G) conformation in the vicinity of one end. The (NH_3^+) groups are linked to the chlorine atoms by three hydrogen bonds with two axial and one equatorial chlorine atoms; this scheme is the only one allowed for steric reasons when $n \geqslant 2$ (Depmeier 1977). Let us note that, in such a configuration, the chains would be approximately perpendicular to the layers if they were all-*trans*. According to structural data (table 2), the value of the interlayer distance *d* in phase III is too short to allow the chains to be in the *trans* configuration and perpendicular to the metallic sheets. So, the longitudinal axis of the cation is tilted with respect to c', which can be obtained only if the *gauche* conformation is located in the vicinity of the ammonium group. The band at 296 cm^{-1} (figure 4) corresponds to the torsional mode of the NH_3 group {$\tau(NH_3)$}.

Table 4. Low-wavenumber Raman lines (10–360 cm^{-1}) observed in phases III, II, II′ and I.

	Phase III 193 K	Phase II 286 K	Phase II′ 304 K	Phase I 320 K	Assignments
ν_1	28 m[a]				$(C_9H_{19}NH_3)^+$
ν_2	48 s[b]	45 s	42 m	41 m	$(C_9H_{19}NH_3)^+$
ν_3	117 vs[c]	96 m	86 m	84 m	$(C_9H_{19}NH_3)^+$
ν_4	134 vs	130 m	124 m	124 m	ν(Pb–Cl)
ν_5	168 m				$(C_9H_{19}NH_3)^+$
ν_6	196 m	190 w[d]	190 w	190 w	$R'(C_9H_{19}NH_3)^+$
ν_7	243 sh	243 sh	243 sh	250 sh	
ν_8	254 sh	254 sh	254 sh		LAM-1
ν_9	296 sh	287 sh	284 sh		$\tau(NH_3)$

[a] Medium.
[b] Strong.
[c] Very strong.
[d] Weak.
[e] Shoulder.

4.1.2. Infrared spectra of C_9Pb at 90 K. In the infrared spectrum between 700 and 1400 cm^{-1} (figure 5) a number of modes correspond to the vibrations which involve the entire chain and give rise to progression bands. Their number, wavenumber and intensity depends on both length and configuration of the chains (Synder and Schachtschneider 1963,

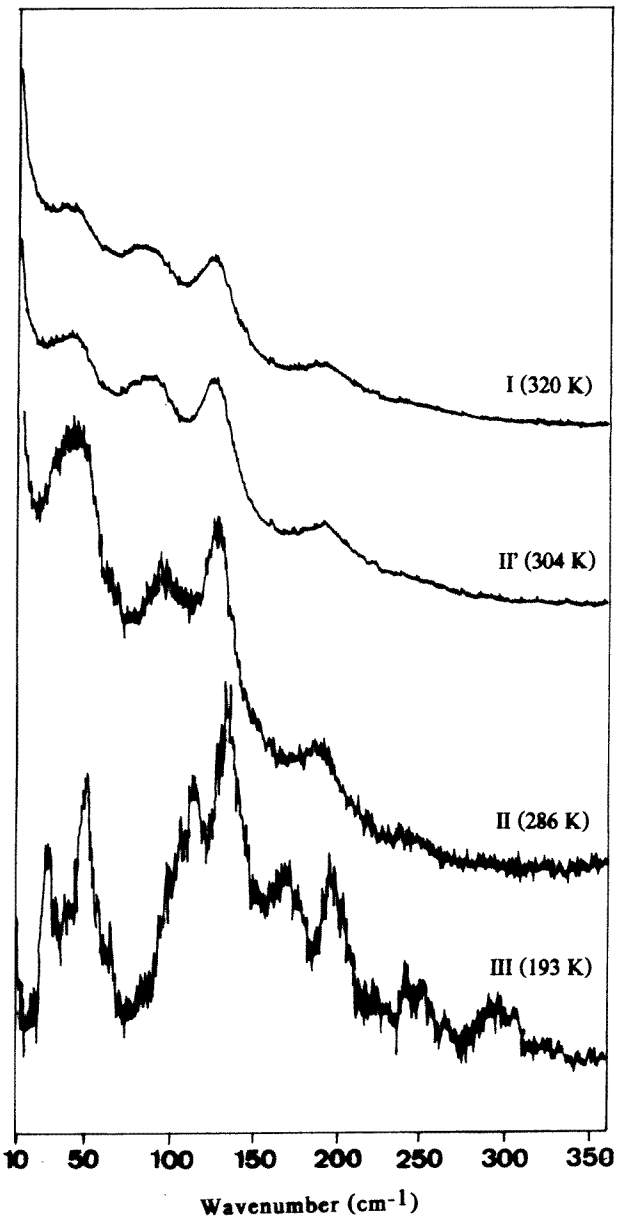

Figure 4. The temperature dependence of the Raman spectrum of $(C_9H_{19}NH_3)_2PbCl_4$ between 10 and 360 cm^{-1}.

Snyder *et al* 1983, Zerbi *et al* 1981). From previous experience in the analysis of the spectra of normal paraffins we know that in the infrared the most characteristic progressions of bands are those associated with the CH_2 rocking and wagging motions (Synder *et al* 1983, Zerbi *et al* 1981). The splitting observed at 723–730 cm^{-1}, which is assigned to the CH_2 rocking

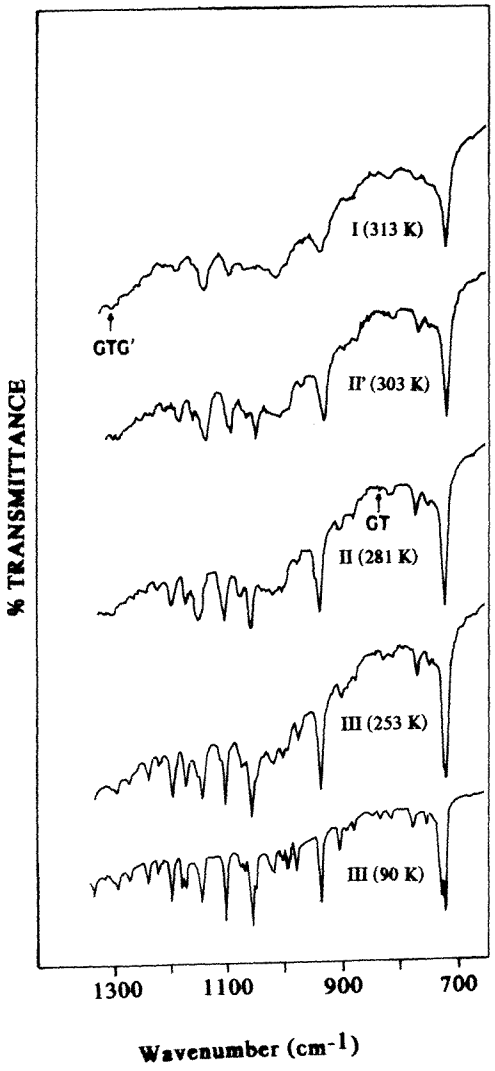

Figure 5. The temperature dependence of the infrared spectrum of $(C_9H_{19}NH_3)_2PbCl_4$ between 700 and 1350 cm^{-1}.

fundamental mode $r(CH_2)$ is due to the crystalline field effect. The progression absorption bands usually attributed to CH_2 wagging modes can be seen in the spectra of crystalline *n*-paraffins in the region 1150–1350 cm^{-1} (Synder 1960). These modes are mixed with the CH_3 and $(NH_3)^+$ internal modes. The coupling with the $(NH_3)^+$ group may be reason for the strong enhancement of the intensity of the CH_2 wagging modes compared with the case of *n*-alkanes (Ricard *et al* 1984).

Raman and infrared spectra of the low-temperature phase III are typical of an ordered solid. The vibrational behaviour gives further evidence for the existence of intermolecular coupling in an almost extended chain.

4.2. Study of the disordered phases

In order to obtain information on the crystal dynamics, on the degree of disorder in different phases and on the mechanisms involved in the transitions, we have undertaken a spectroscopic study of the different disordered phases.

4.2.1. Changes in the Raman spectra for the disordered phases. For Raman spectroscopy, the study is restricted to the low-wavenumber range (10–360 cm^{-1}), because this includes lattice modes and some internal modes which are the most sensitive for crystal changes and phase transitions. The spectral evolution with temperature variation is shown in figure 4.

III → II transition (275 K). When increasing the temperature from phase III to phase II, the spectral modifications concern both modes of the organic chains and modes of $PbCl_6$ octahedra. The intensity of the band at 48 cm^{-1} decreases, then it broadens with the band at 28 cm^{-1}. The wavenumber of the band at 117 cm^{-1} decreases by about 20 cm^{-1}. The band at 134 cm^{-1}, assigned to the $\nu(Pb-Cl)$ mode, is shifted to 130 cm^{-1}. The intensity of this mode decreases while its width increases. Such a behaviour of this dispersive mode in phase II reflects the degree of disorder which is induced in the chlorine lattice. The band at 196 cm^{-1} assigned to chain libration is shifted to 190 cm^{-1}. The wavenumbers of the skeletal deformations are not modified, which indicates that rather extended chains still remain and the number of possible conformers is small. The band assigned to $\tau(NH_3)$ is shifted down to 287 cm^{-1} in phase II; the broadening of this band together with the significant downwards shift of its wavenumber noticed on heating confirms that the NH_3 ends are directly involved in the disordering processes.

II → II′ transition (301.8 K). The spectral evolution across the II → II′ transition can be explained as follows. The band at 96 cm^{-1} decreases by about 10 cm^{-1}. The ν(Pb–Cl) stretching mode is shifted to 124 cm^{-1}. The intensity of this band decreases while its width increases. This behaviour shows the degree of disorder which is induced in the chlorine lattice.

II′ → I transition (308.6 K). On heating the sample from phase II′ to phase I, changes in spectra are characterized as follows. The band of the LAM-1 is replaced with a wider band of which the maximum is at 250 cm^{-1}. This indicates the presence of several not entirely extended conformers. The band assigned to $\tau(NH_3)$ broadens and disappears, which could be due to the onset of flipping of NH_3 polar heads between potential wells.

4.2.2. Changes in the infrared spectra for the disordered phases. Figure 5 shows the evolution of the infrared spectrum versus temperature of C_9Pb.

CH_2 rocking. By increasing the temperature from phase III to phase II, the $r(CH_2)$ doublet structure tends to disappear, and only a singlet at 724 cm^{-1} is observed at 281 K. The infrared spectrum in phase II shows the appearance of a shoulder at 840 cm^{-1}, which reveals the existence of new conformers. In alkanes, the infrared band at 840 cm^{-1} has been shown to be characteristic of *gauche* forms (GT) in the vicinity of the methyl group ($G_{CH_2-CH_3}$) (Zerbi *et al* 1981). When the temperature increases from phase II to phase II' no noticeable discontinuities are observed and the $r(CH_2)$ singlet appears at 723 cm^{-1}. On further heating up to 313 K (phase 1) we observe a slight modification of the bandshape (intensity and bandwidth) of the singlet. It appears at 722 cm^{-1}, which is similar to the band of the CH_2 rocking modes in liquid *n*-alkanes.

CH_2 wagging. By increasing the temperature from phase III to phase II, the intensity of the CH_2 wagging progression bands decreases and their width increases, but they remain as

a prominent feature of this region. This behaviour shows that the features characteristic of fully extended chains are lost. No noticeable changes are observed through the second phase transition II $\rightarrow$ II′ On further heating up to phase I, the progression bands tend to overlap and form a continuous background. The spectrum of phase I shows a spectroscopic feature near 1306 cm^{-1}, which continuously increases in intensity while the other CH_2 waggings decrease. This has been shown in alkanes to be characteristic of GTG′ defects (Synder 1967). We can say that through the II′ $\rightarrow$ I phase transition GTG′ defects are generated and that it takes a wide temperature range to reach a limiting value in the concentration of these defects.

5. Qualitative results and model for phase transitions

We conclude from this study that the III $\rightarrow$ II transition is of the first order–disorder type and involves the orientational and conformational dynamics of the organic chains and deformation of $PbCl_6$ octahedra. The appearance of a new spectroscopic feature involves the conformational disorder of the hydrocarbon chains. Intermolecular interactions are weak. Finally, in phase II, the linkage of the NH_3 heads to the NH–Cl cavity is radically different from that in phase III.

Comparison of the interlayer distance d (table 2) obtained from crystallographic results of phase III and II involves a crystalline contraction at 275 K. Thus, when the kinks are of the type GT in the vicinity of the methyl group ($G_{GH_2-CH_3}$), the chains are shorter but not strongly affected and are kept in an almost extended configuration, which is allowed by the small decrease of the interlayer distance at the transition III $\rightarrow$ II.

As the phase transition observed at 301.8 K on the DSC heating curve involves a weak thermal effect, this transition is not expected to imply any additional conformational disorder. The identity of the infrared spectra of the II and II′ phases at wavenumbers higher than 700 cm^{-1} supports this idea. Thus, the phase transition II $\rightarrow$ II′ does not seem to be related to internal rotations of the chains but probably to a rearrangement of the $PbCl_6$ octahedra in the perovskite plane.

The structure of form I we arrived at from our vibrational study is the result of the generation of some new conformations in the alkylammonium chain. It mainly consists of the introduction of more G forms or kinks. We can conclude that at the transition II′ $\rightarrow$ I chain melting sets in. DSC analysis show that the transformation II′ $\rightarrow$ I presents pretransitional effects.

The phase transition II′ $\rightarrow$ I particularly affects the interlayer distances. The value of d which is equal to 23.85 Å in phase II′, becomes 24.65 Å in phase I (table 2), which corresponds to an increase of 3%. Let us recall that this value corresponds to the distance between two successive mineral layers $(PbCl_4)^{2-}$. This fact can be explained only by the variation of the tilt of the alkylammonium chains with respect to the c' axis perpendicular to the layer. X-ray diffraction is in agreement with spectroscopic study. Effectively the increase in the basal spacing seems to manifest some change in the chain packing. Types of defect occurring in this phase can be specified from both an analysis of the infrared spectrum and packing considerations. Because of the low value of the d parameter determined by x-ray diffraction in phase I, the longitudinal axis of the chains must be tilted in a way which does not allow the presence kinks of type GTG′ (Kind *et al* 1979). Thus, in the highest-temperature phase I, kinks are rather long (that is to say, of the form $GT_{2n+1}G'$ with $n \geqslant 1$).

References

Abid Y, Kamoun M, Daoud A and Ramain F 1990 *J. Raman Spectrosc.* **21** 709
Abid Y, Kamoun M, Daoud A, Romain F and Lautie A 1992 *Phase Transitions* **40** 239
Chapuis G, Arend H and Kind R 1975 *Phys. Status Solidi* a **31** 449
Depmeier W 1977 *Acta Crystallogr.* B **33** 3713
Kind R *et al* 1979 *J. Chem. Phys.* **71** 2118
Minoni G and Zerbi G 1982 *J. Phys. Chem.* **86** 4791
Mizushima S and Simanouti T 1949 *J. Am. Chem. Soc.* **71** 1320
Ricard L, Rey-Lafon M and Biran C 1984 *J. Phys. Chem.* **88** 5614
Romain F, Lautié A, Abid Y and Grabielle Madelmont C 1992 *Thermochim. Acta* **204** 157
Snyder R G 1960 *Mol. Spectrosc.* **4** 411
——1967 *J. Chem. Phys.* **47** 1316
Snyder R G, Maroncelli M, Strauss H L, Elliger L A, Cameron D G, Casal H L and Mantsh H H 1983 *J. Am. Chem. Soc.* **105** 133
Snyder R G and Schachtschneider J H 1963 *Spectrochim. Acta.* **19** 85
Zerbi G, Magni R, Gussoni M, Moritz K H, Bigotto A and Dirlikov S 1981 *J. Chem. Phys.* **75** 3175